Second-harmonic generation with magnetic-field controllability

Sheng Ju,[1,*] Tian-Yi Cai,[1,2] Chi-I Wei,[3] and Guang-Yu Guo[3,4]

[1]*Department of Physics and Jiangsu Key Laboratory of Thin Films, Soochow University, Suzhou 215006, China*
[2]*Department of Physics, The University of Texas, Austin, Texas 78712, USA*
[3]*Department of Physics and Center of Theoretical Sciences, National Taiwan University, Taipei 106, Taiwan*
[4]*Graduate Institute of Applied Physics, National Chengchi University, Taipei 116, Taiwan*
**Corresponding author: jusheng@suda.edu.cn*

Received August 19, 2009; revised October 23, 2009; accepted October 24, 2009;
posted November 10, 2009 (Doc. ID 115910); published December 10, 2009

Based on density functional theory with the generalized gradient approximation plus on-site Coulomb repulsion method, we study the magnetic-ordering dependence of second-harmonic generation (SHG) in a polar magnet $BiCoO_3$. The large second-order optical susceptibility, which can reach 3.7×10^{-7} esu, exhibits a strong magnetic-ordering dependence, giving rise to magnetic-field controllable SHG response in polar magnets. © 2009 Optical Society of America

OCIS codes: 160.2260, 160.4330, 190.2620.

Noncentrosymmetric polar materials are of great interest in material science and engineering, because their symmetry-dependent properties such as ferroelectricity, piezoelectricity, and second-harmonic generation (SHG) are technologically important [1]. In particular, the search for new SHG materials is of current interest for their application in photonic technologies. Generally speaking, in polar materials, the larger spontaneous electric polarization, the stronger the SHG susceptibility [2]. In polar magnets, the magnetic degrees of freedom and its coupling with electric order can lead to some interesting nonlinear optical phenomena [3–7]. In this Letter, we explore SHG in a polar magnet $BiCoO_3$ from first principles. $BiCoO_3$ possesses $PbTiO_3$-like perovskite structure, but with a much larger tetragonality [8]. The electric polarization is predicted to be 150 $\mu C/cm^2$, the largest value among the ever known polar materials [9]. In addition, C-type antiferromagnetic (AFM) ordering is observed in this almost-two-dimensional layered structure. Based on density functional theory, we find that owing to the extremely large tetragonality as well as large electric polarization, $BiCoO_3$ possesses very large SHG susceptibilities. Furthermore, SHG changes dramatically between different magnetic orderings, giving rise to magnetic-field controllable SHG response.

Our *ab initio* calculations are performed using the accurate full-potential projector augmented wave (PAW) method [10], as implemented in the Vienna *ab initio* Simulation Package (VASP) [11–14]. They are based on density functional theory with the generalized gradient approximation (GGA). The on-site Coulomb interaction is included in the GGA+U approach with effective U of 5 eV for Co $3d$ electrons [15]. A large plane-wave cutoff of 500 eV is used throughout, and the convergence criterion for energy is 10^{-6} eV. PAW potentials are used to describe the electron–ion interaction, with 15 valence electrons for Bi ($5d^{10}6s^26p^3$), 9 for Co ($3d^74s^2$), and 6 for O ($2s^2p^4$). The fully relaxed crystal structure [$a=3.75611$ Å, $c=4.83398$ Å, Bi (0,0,0), Co (0.5,0.5,0.5765), $O_\perp$ (0.5,0.5,0.2139) and $O_\parallel$ (0, 0.5, 0.7288)], which shows a $P4mm$ tetragonal symmetry, is in good agreement with experiment data [8]. In present calculations, we consider four types of collinear spin configurations, i.e., C-type AFM ordering (ground state) with $\mathbf{q}=(0.5,0.5,0)$, G-type AFM ordering with $\mathbf{q}=(0.5,0.5,0.5)$, A-type AFM ordering with $\mathbf{q}=(0,0,0.5)$, and ferromagnetic (FM) ordering [16]. Supercells of $\sqrt{2}a\times\sqrt{2}a\times c$, $\sqrt{2}a\times\sqrt{2}a\times2c$, and $a\times a\times2c$ are adopted for C-type, G-type, and A-type, respectively. The Brillouin zone intergrations are performed with the tetrahedron method in a Monkhorst–Pack k-point mesh centered at the Γ point [17]. Total energy indicates that C-type AFM ordering is the ground state, which is consistent with the experimental observation [8].

The optical properties are calculated based on the independent-particle approximation [18–20]. The imaginary part of the dielectric function due to direct interband transitions is given by Fermi golden rule, i.e., $\epsilon''_{aa}=4\pi^2/\Omega\omega^2\Sigma_{i\in VB,j\in CB}\Sigma_{\mathbf{k}}w_{\mathbf{k}}|p^a_{ij}|^2\delta(\epsilon_{\mathbf{k}_j}-\epsilon_{\mathbf{k}_i}-\omega)$, where Ω is the unit-cell volume and ω is the photon energy. VB and CB denote the conduction and valence bands, respectively. The dipolar transition matrix elements $p^a_{ij}=\langle\mathbf{k}_j|p_a|\mathbf{k}_i\rangle$ are obtained from the self-consistent band structures within the PAW formalism. Here $|\mathbf{k}_n\rangle$ is the nth Bloch-state wave function with crystal momentum $\mathbf{k}$ and a denotes the Cartesian component. The real part of the dielectric function is obtained from ϵ'' by a Kramers–Kronig transformation $\epsilon'(\omega)=1+2/\pi\mathbf{P}\int_0^\infty d\omega\omega'\epsilon''(\omega')/\omega'^2-\omega^2$. Here $\mathbf{P}$ is the principle value of the integral.

The imaginary part of the second-order optical susceptibility due to direct interband transitions is given by $\chi''^{(2)}_{abc}(-2\omega,\omega,\omega)=\chi''^{(2)}_{abc,VE}(-2\omega,\omega,\omega)+\chi''^{(2)}_{abc,VH}\times(-2\omega,\omega,\omega)$ [21], where the contribution due to the so-called virtual-electron process $\chi''^{(2)}_{abc,VE}$ and that due to the virtual-hole process $\chi''^{(2)}_{abc,VH}$ are included [20]. The real part of the second-order optical susceptibility is then obtained from the imaginary part by a

Kramers–Kronig transformation $\chi'^{(2)}(-2\omega,\omega,\omega) = 2/\pi \mathbf{P}\int_0^\infty d\omega' \omega' \chi'^{(2)}(2\omega',\omega',\omega')/\omega' 2 - \omega^2$. In calculations, the δ functions are approximated by a Gaussian function with $\Gamma = 0.1$ eV. We use a dense grid of k points (e.g., $16\times16\times18$ with 450 total irreducible k points for C-type AFM $BiCoO_3$), 20 bands per atom, and the 50 eV of the maximum energy in the integrals of real part of ϵ and $\chi^{(2)}$ to guarantee the accuracy of the present optical calculations.

For the $P4mm$ crystal symmetry and collinear magnetic ordering of $BiCoO_3$, there are three components of linear dielectric function: ϵ_{xx}, ϵ_{yy}, and ϵ_{zz}, with $\epsilon_{xx} = \epsilon_{yy}$ [22]. For the SHG susceptibilities, there are five nonvanishing components, with $\chi^{(2)}_{xxz} = \chi^{(2)}_{yyz}$; $\chi^{(2)}_{zxx} = \chi^{(2)}_{zyy}$; and $\chi^{(2)}_{zzz}$ [22]. As shown in Fig. 1, there is a little difference in ϵ among four types of magnetic orderings. In particular, at low frequency, linear optical response is almost identical with each other. However, SHG coefficients display great contrast between each other in the whole frequency range we demonstrated. As indicated in Table 1, the change in the low

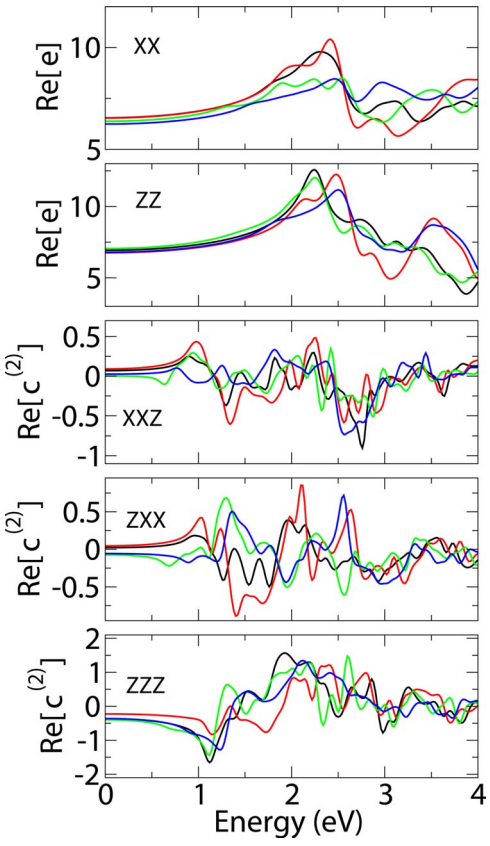

Fig. 1. (Color online) Magnetic-ordering dependence of linear dielectric function and SHG (10^{-6} esu) in $BiCoO_3$ (real part). For xx component, the sequence at low frequency (in the ascending sort) is FM, A-type AFM, G-type AFM, and C-type AFM. For zz component, the sequence is G-type AFM, FM, C-type AFM, and A-type AFM. For xxz component, the sequence is A-type AFM, FM, C-type AFM, and G-type AFM. For zxx component, the sequence is A-type AFM, FM, C-type AFM, and G-type AFM. For zzz component, the sequence is A-type AFM, C-type AFM, FM, and G-type AFM.

Table 1. Magnetic-Ordering Dependence of Linear Dielectric Constant (ϵ_∞) and Low-Frequency Second-Order Susceptibility ($\chi^{(2)}$) (10^{-8} esu) in $BiCoO_3$

	C-Type AFM	G-Type AFM	A-Type AFM	FM
ϵ_{xx}	6.55	6.54	6.38	6.24
ϵ_{zz}	6.93	6.76	7.05	6.79
$\chi^{(2)}_{xxz}$	6.9	9.05	0.29	2.57
$\chi^{(2)}_{zxx}$	2.19	4.56	−7.36	−5.65
$\chi^{(2)}_{zzz}$	−36.86	−22.59	−39.69	−36.24

frequency SHG is more obvious. In particular, there is a more than 50% change in $\chi^{(2)}_{xxz}$ and $\chi^{(2)}_{zxx}$ between C-type AFM state and FM state. Such a large change in SHG can be observed directly by the application of external magnetic field when the system transforms from C-AFM ground state to FM state or the suppression of spin fluctuation at finite temperature. The magnetic field needed for the zero-temperature C-AFM ground state to FM state transition is very large, around 60 T. However, the magnetic ordering and spin-pair correlation are also affected by temperature. In particular, near Neel temperature, the spin-pair correlation shows the strongest magnetic-field dependence, and therefore SHG can exhibit obvious magnetic-field dependence near Neel temperature. In addition, SHG susceptibility itself is large. For example, the low-frequency $\chi^{(2)}_{zzz}$ reaches as high as 3.7×10^{-7} esu, almost five times larger than SHG in $LiNbO_3$, which is a typical nonlinear optical material. The large SHG is consistent with the large polar distortion and electric polarization in $BiCoO_3$.

To understand the above large change of SHG microscopically, in Fig. 2 we plot the absolute value of imaginary part of $\chi^{(2)}$ in contrast with $\epsilon''(\omega)$ and $\epsilon''(\omega/2)$. First, we can find that SHG spectrum can be divided into three regions: the regime within $\hbar\omega$

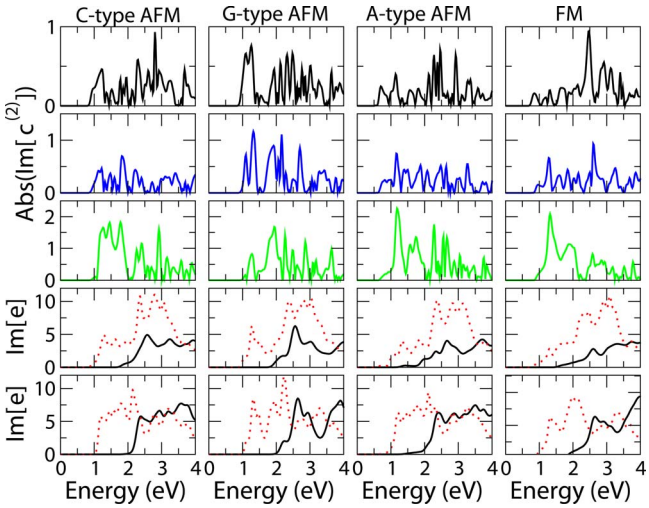

Fig. 2. (Color online) Magnetic-ordering dependence of linear dielectric function and SHG (10^{-6} esu) in $BiCoO_3$ (imaginary part). From the top to the bottom are the components of $\chi^{(2)}_{xxz}$, $\chi^{(2)}_{zxx}$, $\chi^{(2)}_{zzz}$, ϵ_{xx}, and ϵ_{zz}. The dotted line is for $\epsilon''(\omega/2)$, and solid line is for $\epsilon''(\omega)$.

$\leqslant 2$ eV, corresponding the double-photon resonance; the regime within $2\ \text{eV} \leqslant \hbar\omega \leqslant 3$ eV, corresponding the joint double-photon and single-photon resonances; and the regime beyond, corresponding to the single-photon resonance. Second, it is noted that C-type AFM state and A-type AFM state resemble each other in linear optical absorption peaks, while G-type AFM state and FM fall into the same group. Between C-type AFM state and FM state, both $\epsilon''(\omega)$ and $\epsilon''(\omega/2)$ differ greatly. The difference is further amplified in double-photon resonance region of SHG spectrum ($\hbar\omega \leqslant 2$ eV), where $\chi''^{(2)}$ differs significantly in the absorption peaks' height between four different magnetic orderings. Therefore, the large change in SHG arises mainly from enhanced contrast in the double-photon resonance absorption.

In applications, such an obvious change in SHG is useful. The conventional electro-optic effect, which is related to the magnitude of low-frequency second-order optical susceptibility and measures the change of linear optical response under external electric field, will also be magnetic-field (or magnetic-ordering) dependent. Therefore a novel magneto-electro-optic effect can be observed in polar magnets.

From the above calculations, strong magnetic-ordering dependence of SHG is well established in the polar magnet $BiCoO_3$. Magnetic-ordering-dependent SHG similar to those described above should be general in all the polar magnets. In fact, consistent with the suggestion by Tokura [7], these conventional polar magnets can show very interesting linear and nonlinear optical properties arising from the magnetoelectric response in the optical-frequency region, yet the coupling between electric polarization and magnetization at their electronic ground state appears to remain very small. On the other hand, complex modification of SHG (both the magnitude and the number of components) in the improper ferroelectric materials is possible [4], since the spontaneous electric polarization in these improper ferroelectric materials is associated with the particular noncollinear magnetic ordering. In these materials, the spontaneous electric polarization itself is magnetic-ordering dependent, so $\chi^{(2)}$ will change strongly with external magnetic field. It is noted that the magnetic-field controllable SHG is intrinsic in these polar magnets. This is different with the extrinsic effects in the composite materials, where the composite microstructure is magnetic-field dependent [23].

In summary, by examining the magnetic-ordering dependence of nonlinear optical response, we have revealed the magnetic-field controllable SHG in a layered polar magnet $BiCoO_3$. Large SHG susceptibility, which can reach 3.7×10^{-7} esu, undergoes a substantial change between different magnetic orderings. Novel optical phenomena of magnetic-field controllable SHG and magneto-electro-optic effect are therefore realized in polar magnets.

The authors gratefully acknowledge supports from the National Natural Science Foundation of China (NSFC) under grant 10974140, National Science Council of Taiwan (NSCT), and National Center for Theoretical Sciences of Taiwan.

References

1. P. S. Halasyamani and K. R. Poppelmeier, Chem. Mater. **10**, 2753 (1998).
2. S. Ju and G. Y. Guo, J. Chem. Phys. **129**, 194704 (2008).
3. D. Sa, R. Valenti, and C. Gros, Eur. Phys. J. B **14**, 301 (2000).
4. M. Fiebig, V. V. Pavlov, and R. V. Pisarev, J. Opt. Soc. Am. B **22**, 96 (2005).
5. Y. Shimada, M. Matsubara, Y. Kaneko, J. P. He, and Y. Tokura, Appl. Phys. Lett. **89**, 101112 (2006).
6. E. Hanamura and Y. Tanabe, Phase Transitions **79**, 957 (2006).
7. Y. Tokura, J. Magn. Magn. Mater. **310**, 1145 (2007).
8. A. A. Belik, S. Iikubo, K. Kodama, N. Igawa, S. Shamoto, S. Niitaka, M. Azuma, Y. Shimakawa, M. Takano, F. Izumi, and E. Takayama-Muromachi, Chem. Mater. **18**, 798 (2006).
9. Y. Uratani, T. Shishidou, F. Ishii, and T. Oguchi, Jpn. J. Appl. Phys. Part 1 **44**, 7130 (2005).
10. P. E. Blochl, Phys. Rev. B **50**, 17953 (1994).
11. G. Kresse and J. Hafner, Phys. Rev. B **47**, 558 (1993).
12. G. Kresse and J. Hafner, Phys. Rev. B **49**, 14251 (1994).
13. G. Kresse and J. Furthmuller, Comput. Mater. Sci. **6**, 15 (1996).
14. G. Kresse and D. Joubert, Phys. Rev. B **59**, 1758 (1999).
15. S. L. Dudarev, G. A. Botton, S. Y. Savrasov, C. J. Humphreys, and A. P. Sutton, Phys. Rev. B **57**, 1505 (1998).
16. J. Goodenough, Phys. Rev. **100**, 564 (1955).
17. P. E. Blochl, O. Jepsen, and O. K. Andersen, Phys. Rev. B **49**, 16223 (1994).
18. G. Y. Guo, K. C. Chu, D. S. Wang, and C. G. Duan, Phys. Rev. B **69**, 205416 (2004).
19. G. Y. Guo and J. C. Lin, Phys. Rev. B **71**, 165402 (2005).
20. G. Y. Guo and J. C. Lin, Phys. Rev. B **72**, 075416 (2005).
21. D. E. Aspnes, Phys. Rev. B **6**, 4648 (1972).
22. R. W. Boyd, *Nonlinear Optics* (Elsevier, 2003).
23. C. Z. Fan and J. P. Huang, Appl. Phys. Lett. **89**, 141906 (2006).